Research Square

Preprints are preliminary reports that have not undergone peer review.
They should not be considered conclusive, used to inform clinical practice,
or referenced by the media as validated information.

The Utilization of Ultrasonic Characteristics for Identifying Precursors of Low-Cycle Fatigue Crack Formation in AA5083 Aluminum

Hsuan-Han Lai
National Chung Hsing University
En Hong Zhou
National Chung Hsing University
Chi-Ming Lin
National Chung Hsing University
Chao Hui Ou
National Kaohsiung University of Science and Technology
Yun-His Chao
Hong Wen International School
Weite Wu
wwu@dragon.nchu.edu.tw
National Chung Hsing University

Research Article

Keywords: fatigue crack, nonlinear ultrasonics, sideband peak count index (SPC-I), residual stress, X-ray FWHM

Posted Date: May 27th, 2026

DOI: https://doi.org/10.21203/rs.3.rs-8974042/v1

License: This work is licensed under a Creative Commons Attribution 4.0 International License.
Read Full License

Additional Declarations: No competing interests reported.

Version of Record: A version of this preprint was published at Journal of Nondestructive Evaluation on October 11th, 2026. See the published version at https://doi.org/10.1007/s10921-026-01442-7.

The Utilization of Ultrasonic Characteristics for Identifying Precursors of Low-Cycle Fatigue Crack Formation in AA5083 Aluminum.

Hsuan-Han Lai [1], En Hong Zhou [1], Chi-Ming Lin [2], Chao Hui Ou [3], Yun-His Chao [4], Weite Wu [1*]

1. Department of Materials Science and Engineering, National Chung Hsing University, No. 145, Xingda Road, South Dist., Taichung City, 402202, Taiwan, R.O.C.

2. Academy of Circular Economy, National Chung Hsing University, No. 15, Guangming Rd., Nantou City, Nantou County, 540, Taiwan.

3. Department of Mold and Die Engineering, National Kaohsiung University of Science and Technology, No. 415, Jiangong Road, Sanmin Dist., Kaohsiung City, 807618, Taiwan, R.O.C.

4. Hong Wen International School, No. 100, Hongwen St., Tanzi Dist., Taichung City 427009 , Taiwan (R.O.C.)

Abstract

This study investigates the aluminum alloy AA5083-H112 through low-cycle fatigue testing, employing both linear and nonlinear ultrasonic analysis methods in conjunction with X-ray diffraction analysis and optical microscopy. The objective is to examine the micro-damage evolution preceding fatigue crack initiation and to assess the sensitivity and efficacy of various nondestructive testing indicators for detecting fatigue damage. During the early stages of fatigue, both residual stress and full width at half maximum (FWHM) progressively increase in correlation with the accumulation of dislocations. However, as crack initiation and propagation occur, residual stress and FWHM decrease sharply during the mid-to-late fatigue stages. While acoustic velocity demonstrates significant changes in the initial fatigue stage, subsequent variations are comparatively minor. The RMS amplitude, and the time of flight (TOF) exhibit substantial changes predominantly in the later stages of fatigue. The nonlinear ultrasonic sideband peak counts index (SPC-I) exhibits a pronounced response during the initial fatigue stage, specifically the microcrack initiation phase, thereby demonstrating a high sensitivity for the early detection of fatigue damage.

Keywords: fatigue crack; nonlinear ultrasonics; sideband peak count index (SPC-I); residual stress; X-ray FWHM

***Corresponding author (Weite Wu)**

E-mail address: wwu@dragon.nchu.edu.tw

Tel.: +886-4-22840500#604

Fax: +886-4-2285701

1. Introduction

Fatigue cracks account for up to 90% of failures in metal structures, with such failures frequently occurring without any visible deformations or indicators prior to the event [1]. Consequently, structural health monitoring has become a vital area of research [2]. Common nondestructive testing (NDT) techniques include ultrasonic testing, radiography, magnetic particle inspection, and liquid penetrant testing. Among these methods, ultrasonic testing is particularly advantageous due to its strong penetration capabilities, non-radioactive nature, and applicability across a wide range of materials. It is highly effective in accurately detecting and locating defects and is widely utilized for identifying material flaws and cracks.

Ultrasonic testing can be classified into linear and nonlinear analyses, both of which are based on the acoustoelastic principle. Linear ultrasonic analysis has been extensively studied [3-5] and generally involves quantifying the energy of reflected, scattered, transmitted, and absorbed signals to assess the degree of material damage. Commonly used parameters include sound velocity and amplitude attenuation: sound velocity is determined by measuring the difference in acoustic transmission time, while attenuation is calculated by comparing changes in wave intensity or amplitude. Linear ultrasonic analysis techniques are relatively cost-effective and facilitate rapid detection of macroscopic cracks and voids that have already developed. However, prior to crack formation, microcracks and dislocations are significantly smaller than the ultrasonic wavelength, rendering traditional linear analysis ineffective for their detection. These minute defects often arise during the early stages of fatigue and static tensile processes. Lissenden [6] observed that when traditional linear ultrasonic analysis can detect macroscopic cracks, the material is typically in the late fatigue stage and is at imminent risk of fracture.

Nonlinear ultrasonic analysis provides enhanced sensitivity for detecting

microscopic damage in materials during the early stages of fatigue, thereby enabling earlier diagnosis. To facilitate the early identification of internal damage accumulation, various nonlinear ultrasonic techniques have been developed, including high-harmonic generation (HHG) [7-9], nonlinear wave modulation spectroscopy (NWMS) [10-12], and nonlinear resonant ultrasound spectroscopy (NRUS) [13-15]. HHG typically derives nonlinear parameters by calculating the ratio of the second harmonic amplitude to that of the square of the fundamental wave. This technique demonstrates exceptional sensitivity; however, it requires high-voltage excitation to achieve markedly improved sensitivity, particularly in thick or highly attenuative materials. Additionally, the presence of distinct heterogeneous phases within the material or the use of tubular or rod-shaped specimens may introduce dispersion effects that influence harmonic generation and sensitivity. NWMS employs two ultrasonic waves of differing frequencies to excite the material and detects modulation waves arising in damaged regions, which result from the opening and closing of cracks. This method generally necessitates frequency sweeping to identify the optimal frequency combination, thereby enhancing detection sensitivity. NRUS induces resonance wave within the material through frequency sweeping and monitors nonlinear responses at the resonant frequency, including shifts in resonance frequency, variations in resonance amplitude, and the generation of subharmonics and higher-order harmonics. These nonlinear responses effectively reveal microscopic damage, such as cracks or heterogeneous stress fields. Recent studies have increasingly demonstrated that these nonlinear ultrasonic techniques possess unparalleled potential, particularly for detecting small, early-stage damage. Moreover, these methods exhibit sensitivity that significantly surpasses that of traditional linear analysis techniques, offering more reliable and precise tools for material damage detection.

In nonlinear ultrasonic analysis, defects serve not only as passive scattering centers

but also as active nonlinear sources that generate new frequency components. As ultrasound propagates through damaged materials, it disturbs the stress equilibrium of dislocation accumulations, inducing forced vibrations of dislocations and thereby producing harmonic frequencies [16]. Moreover, ultrasound induces the repeated opening and closing of microcracks - a phenomenon known as "breathing" or "clapping" [17] - which generates waves at frequencies different from the fundamental frequency.

To quantify the nonlinear response of damaged materials and assess their damage states, a novel nonlinear parameter termed the sideband peak count (SPC) was developed recently. The SPC technique does not necessitate a higher harmonic to be generated[18], and it has been applied on different materials for monitoring defects [3, 19, 20]. The SPC is defined as the ratio of the number of signal peaks exceeding a specified threshold to the total number of peaks. Subsequently, the average SPC across all thresholds is calculated to obtain the sideband peak count index (SPC-I) [21], which is a single number that denotes the degree of material nonlinearity [3]. This data processing approach for SPC-I has been successfully applied in the analysis of defects in concrete, metals, and polymer composites [18, 22, 23].

The present study aims to enhance the sensitivity of nonlinear ultrasonic analysis by employing the broadband longitudinal wave excitation SPC-I technique, to compare its performance with other structural health monitoring methods, and to achieve a more comprehensive understanding of micro-defect accumulation in aluminum alloy 5083-H112 at various stages of fatigue. Additionally, this study targets the critical refracted longitudinal wave (LCR wave) for monitoring purposes. The LCR refracts at the material's surface upon entering the material and propagated through the material surface [24]. The selection of LCR is justified by two considerations: first, longitudinal waves generate stronger compressive stresses, thereby increasing sensitivity to defect

sites; second, fatigue cracks predominantly initiate at the surface (except in cases involving internal impurities or other defects), making surface crack monitoring particularly crucial. Since the critical refracted wave propagates along the specimen's surface, it is expected that the LCR wave will demonstrate pronounced nonlinear effects during material inspection.

2. Experiments

This study selected the aluminum alloy AA5083-H112 for low-cycle fatigue testing. Residual stress and the full width at half maximum (FWHM) were analyzed using X-ray diffraction techniques, while optical microscopy was employed to observe and verify the processes of crack initiation and propagation, supplemented by ultrasonic testing. The investigation focused on changes in material properties and microscopic damage behavior preceding fatigue crack initiation. Both linear and nonlinear ultrasonic analysis methods were utilized. Linear ultrasonic analysis employed a pulse-echo transducer; by monitoring variations in sound velocity and signal amplitude attenuation, the degradation of the material's elastic properties was assessed. For nonlinear analysis, a broadband LCR wave was used. The SPC method was applied to the frequency spectrum to calculate the SPC-I as a nonlinear damage parameter, while the time of flight (TOF) of the LCR wave was simultaneously recorded. Through cross-validation of multiple indicators, the microscopic damage mechanisms of the material prior to fatigue crack formation were comprehensively examined.

The experimental material, AA5083, is an aluminum-magnesium alloy characterized by high strength, corrosion resistance, and superior mechanical properties. It exhibits notable resistance to seawater corrosion and excellent weldability, making it widely

employed in engineering sectors such as shipbuilding and transportation manufacturing. Due to its stable structural behavior under fatigue and deformation conditions, AA5083 is particularly well-suited for studies related to fatigue damage and nondestructive testing. The chemical composition of the raw material includes 4.54 wt.% Mg, 0.74 wt.% Mn, and 0.3 wt.% Fe, with the balance being aluminum. Specimens were designed in accordance with ASTM E8/E8M standards, with dimensions depicted in Fig. 1 and a plate thickness of 4 mm.

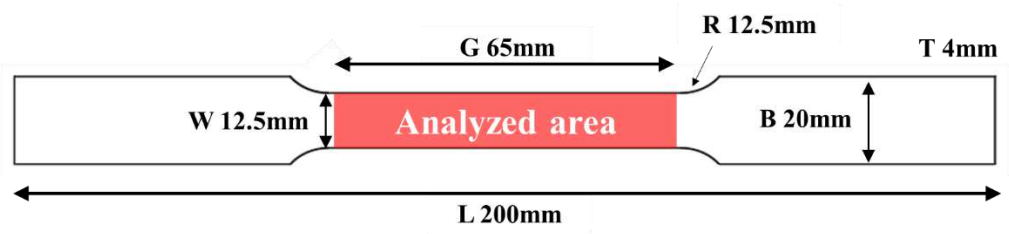


Fig. 1 The specimen illustration of this study.

This study examines the influence of early-stage micro-fatigue damage on the acoustic properties of materials. Considering the high sensitivity of ultrasonic analysis techniques for detecting surface damage, the fatigue test was specifically designed to emphasize a surface-dominated low-cycle fatigue mechanism. Accordingly, the applied stress amplitude was set near the yield strength of the AA5083-H112 aluminum alloy. This approach promotes rapid progression into the plastic deformation stage within a brief period and effectively accelerates the initiation of microcracks as well as enhances the detectability of surface damage, thereby meeting the study's objectives for sensitive detection of early fatigue damage. Specimens were initially subjected to tensile testing to determine the material's yield strength and ultimate tensile strength, which informed the parameters for subsequent fatigue loading. The tensile tests were conducted using a

universal testing machine (model CY-6040) under uniaxial tension at a displacement rate of 0.5 mm/min. Fatigue tests were performed using a servo-hydraulic testing machine (model CY-6676), applying fully reversed cyclic loading with a stress ratio of R = -1 and a loading frequency of 1 Hz.

This study employed a Proto-iXRD X-ray stress analyzer and utilized the $\sin^2\Psi$ method to measure residual stress and analyze the full width at half maximum (FWHM). The detailed procedures were consistent with those described in the previous study [25]. The parameters used for stress analysis included the {311} lattice plane of the α-Al phase, which corresponds to a Bragg angle of 139°, a Young's modulus (E) of 68.9 GPa, a Poisson's ratio (ν) of 0.33, and an X-ray wavelength of 2.29 Å.

The ultrasonic instrument utilized in this study was a Jianwei Technology USG ultrasonic stress analyzer, which incorporated both a combined pulse-echo transducer and a pitch-catch transducer. The pulse-echo transducer, employed in linear measurement techniques as depicted in Fig. 2 , integrates transmitting and receiving functions within a single unit, making it effective for detecting surface and near-surface defects. The transducer operates at a frequency of 5 MHz. It is important to acknowledge that high-frequency sensors possess relatively limited penetration capabilities, and signals may experience significant attenuation when passing through thick or highly attenuating materials. The sensor’s piezoelectric crystal is designed as a circular thin plate with a diameter of 6 mm, conforming to common standard specifications. This dimension optimally balances resolution and signal energy, thereby facilitating stable acoustic wave transmission and reception. Consequently, this sensor design is widely employed in various engineering applications, including metal material inspection and stress evaluation. The methodology for measuring acoustic velocity is illustrated in Fig. 2. Carboxymethyl cellulose (CMC) was uniformly applied to the specimen surface as a coupling agent during measurement. This method

determines the time difference between the reflected waves from the surface and the bottom, combined with the known sample thickness, to estimate the acoustic velocity. However, the samples used in this study have a thickness of only 4 mm, resulting in a very short time interval between the surface reflection and the first bottom reflection wave. This short interval complicates the precise identification of the surface echo arrival time. Therefore, the present experiment employs the analytical approach depicted in Fig. 3, which utilizes the time difference between the first and second clearly defined reflected waves for calculation. Since both of these waves are reflections from the bottom of the material and the time interval between them is longer, this method substantially improves the accuracy of the time difference measurement. The formula for calculating the acoustic velocity (v) is provided below:

$$v=\frac{2d}{t_{b_2}-t_{b_1}} \qquad \text{eq. 1}$$

where d is the sample thickness (4 mm), t_{b1} and t_{b2} are the arrival times of the first and second reflection, respectively.

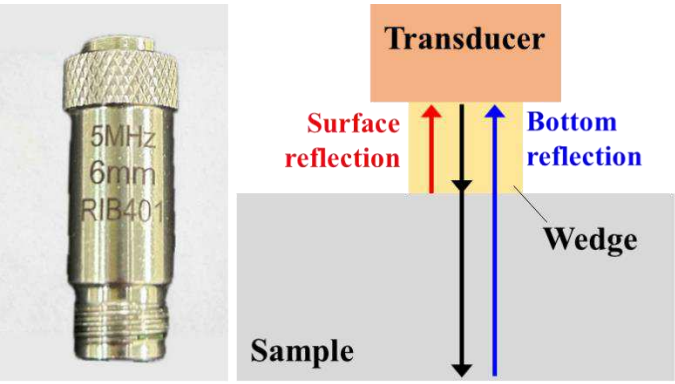


Fig. 2 The pulse-echo transducer and the illustration of acoustic wave reflection.

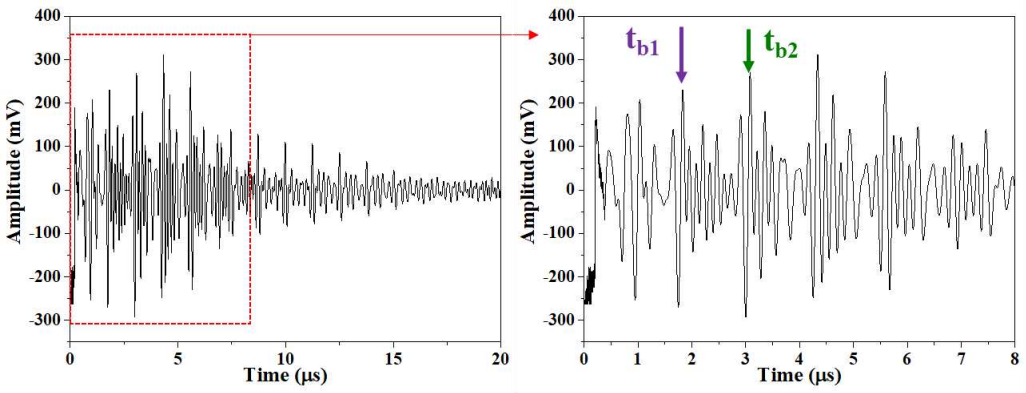


Fig. 3 The waveform detected by the pulse-echo transducer

The waveform detected by the pulse-echo transducer was utilized for amplitude attenuation analysis. To accurately analyze ultrasonic amplitude attenuation, this study excludes waveforms occurring prior to 1.5 μs, retaining only the actual echo signals for processing. Following ultrasonic excitation, initial signals are often affected by pre-trigger noise, which may originate from electronic interference during sensor activation, instability during amplifier startup, or initial micro-vibrations at the interface between the probe and the test specimen. This noise is unrelated to the true echoes within the material and, if not excluded, could compromise the accuracy of amplitude analysis. Although six distinct echo signals are identifiable in the time-domain waveform shown in Fig. 3, the energy of the sound waves gradually attenuates as they propagate within the material. Therefore, this study selects the first three stable echoes with higher amplitudes for subsequent analysis to ensure signal quality and data reliability. Amplitude attenuation is quantified using the root mean square (RMS) value as an amplitude index. The RMS value effectively represents the average energy intensity within a segment of the signal, providing both stability and sensitivity for characterizing amplitude variations. The formula for calculating RMS is presented as follows:

$$RMS=\sqrt{\frac{1}{N}\sum_{i=1}^{N} x_i^2} \qquad \text{eq. 2}$$

Fig. 4 depicts the pitch-catch transducer configuration used for the analysis of the LCR wave. The setup includes a probe with a 22° acoustic incident angle and a fixed separation of 20 mm between the transmitter and receiver, both embedded within a PMMA wedge. The transmitter generates an acoustic wave at a frequency of 5 MHz. Carboxymethyl cellulose was also applied to the specimen surface as a coupling agent. Additionally, Fig. 4 presents the acoustic waveform of the LCR. The LCR sensitively reflects variations in acoustic wave propagation characteristics caused by changes in the internal microstructure of the material during fatigue damage accumulation. The analysis of LCR waves is conducted by comparing the time of flight (TOF) of the refracted waves. Moreover, this study incorporates the SPC method for nonlinear signal analysis, thereby providing a more comprehensive and quantitative assessment of the nonlinear acoustic features associated with the initiation and progression of microcracks at different stages of fatigue.

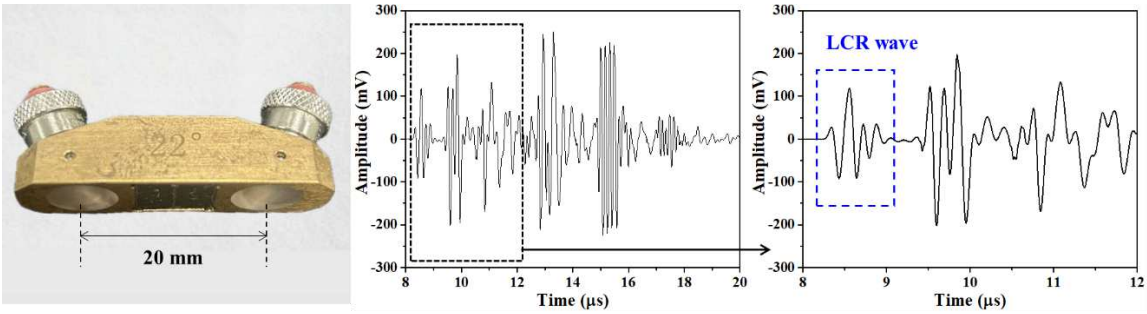


Fig. 4 The pitch-catch transducer and the illustration of LCR wave.

This study utilizes the sideband peak count (SPC) method to analyze acoustic waves measured via the critical refraction wave LCR, employing it as an evaluative

index to quantify the nonlinear behavior of ultrasound. Initially, acoustic waves within the 8 to 12 μs interval of the time-domain signal, as illustrated in Fig. 4, are selected for analysis; this interval includes the critical refraction wave LCR as well as multiple internal reflection signals within the material. A Fourier transform is performed using the Python programming language to convert the original time-domain signal into the frequency domain, yielding the spectral data presented in Fig. 5. To enhance the comparability and stability of results across different samples, the spectral signals are normalized by standardizing the maximum peak intensity in the frequency domain to unity. This normalization effectively reduces amplitude variations caused by external factors such as instrument sensitivity or coupling efficiency during measurement. Furthermore, Fig. 5 identifies the peak positions of all significant frequency components to facilitate subsequent statistical analyses and calculations.

Traditional sideband peak count (SPC) methods generally assess damage by counting the number of frequency peaks that exceed a predetermined amplitude threshold. However, when the total number of peaks varies significantly across samples, this approach may introduce evaluation bias. To overcome this limitation, the present study proposes an enhanced SPC index, defined as the ratio of the number of peaks above a specified threshold ($N_{Peak(th)}$) to the total number of peaks ($N_{Peak(total)}$), thereby quantifying the "proportion of nonlinear components" within the spectrum. This modification effectively reduces statistical errors caused by variations in total peak counts among samples, thereby improving the stability and reliability of the nonlinear response index. The formula for calculating the improved SPC value at a given threshold ($SPC_{(th)}$) is provided in eq. 3.

$$SPC_{(th)} = \frac{N_{Peak(th)}}{N_{Peak(total)}} \qquad \text{eq.3}$$

To reduce erroneous peak identification caused by low-level noise, the lower limit of the SPC threshold is set at 1% amplitude (0.01) of the highest spectral peak. This method effectively eliminates low-amplitude false peaks generated by noise from affecting the statistical analysis. Additionally, this study calculates multiple $SPC_{(th)}$ values by varying the threshold settings and subsequently averages these values to obtain a more representative metric, termed the SPC-I, which serves as the evaluation index for the material's nonlinear response. The corresponding calculation is provided in eq. 4, where $N_{(th)}$ represents the number of thresholds used (rather than the threshold values themselves). It was suggested that $N_{(th)}$ should be at least 20 [18, 20]. In this study, thresholds range from a minimum of 0.01 to a maximum of 1, encompassing a total of 100 discrete threshold levels, for carefully consideration.

$$\text{SPC-I}=\frac{\Sigma SPC_{(th)}}{N_{(th)}} \qquad \text{eq.4}$$

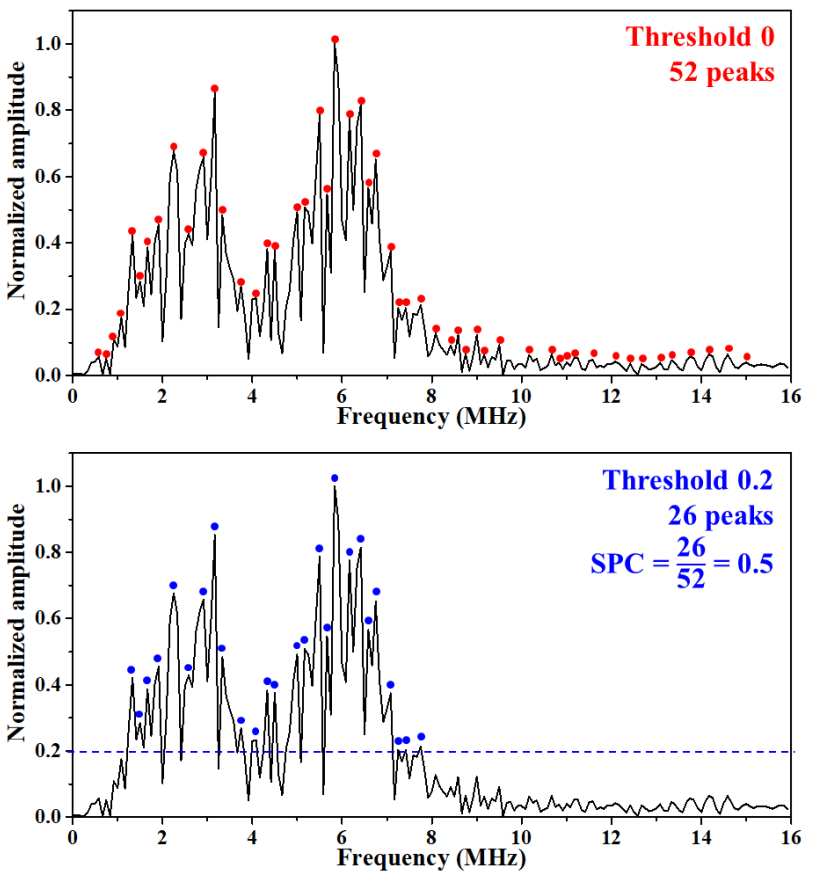


Fig. 5 The frequency spectrum of the wave from pitch-catch transducer, and the acquiring of SPC.

3. Results and discussion

To assess the fundamental mechanical properties and fatigue behavior of the AA5083-H112 aluminum alloy, uniaxial tensile tests were initially conducted to obtain the complete stress-strain curve of the material. Fig. 6(a) presents the results of these tensile tests, which revealed a yield strength of 153 MPa and an ultimate tensile strength of 275 MPa. These mechanical properties suggest that AA5083-H112 possesses notable work hardening capacity and considerable ductility, thereby fulfilling critical requirements for high strength and corrosion resistance in engineering applications. The tensile curve indicates a stable linear elastic response, followed by a pronounced work

hardening effect during the onset of plastic deformation, culminating in fracture at the ultimate tensile strength. It is important to note that AA5083-H112, an aluminum-magnesium alloy, contains a high density of dislocations and solid solution strengthening elements within its microstructure. During tensile testing, dislocation slip and accumulation play a significant role in determining the material's strength and ductility. Nevertheless, this study primarily concentrates on fatigue damage accumulation and the evaluation of non-destructive testing methods, thus only briefly addressing microstructural strengthening mechanisms, such as dislocation atmospheres, without an in-depth investigation of microstructural evolution. To further analyze fatigue behavior, a fixed stress cycle load corresponding to the yield stress of 153 MPa was applied in short-cycle fatigue tests using a tensile-compressive symmetric loading cycle with an R ratio of -1. The fatigue load was repeatedly applied at a constant stress amplitude until specimen failure occurred. The results of the constant load fatigue test, shown in Fig. 6(b), indicate a fatigue life of approximately 5000 cycles.

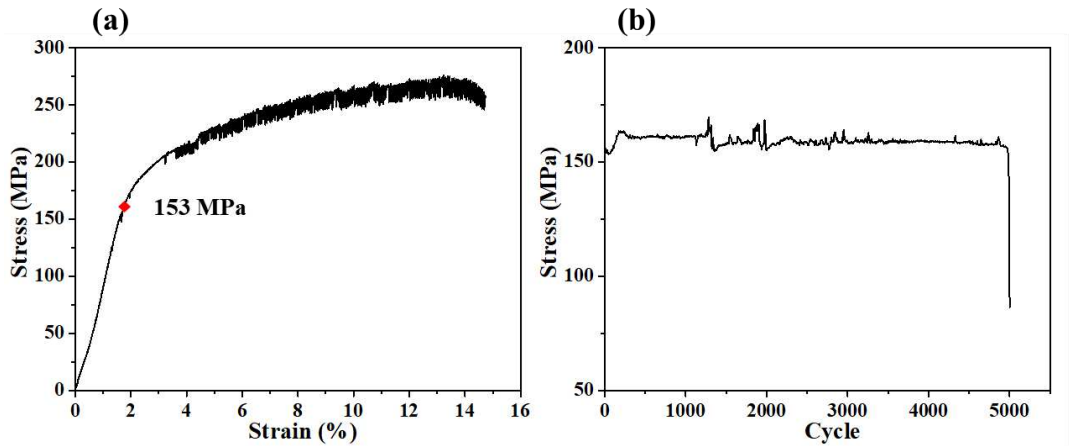


Fig. 6 (a) Sample tensile test stress strain curve; (b) loading cycle of the sample.

This study utilized X-ray stress analysis equipment to systematically monitor

changes in surface residual stress of the specimen during cyclic loading at predetermined cycle intervals. Fig. 7(a) depicts the evolution of material residual stress as a function of fatigue cycles. Initially, at zero cycles, the surface residual stress was measured at -9.72 MPa, attributable to the cold processing of the raw material. With increasing fatigue cycles, the surface residual stress shifted from a compressive to a tensile state, reaching a maximum value of 52.47 MPa at 2200 cycles. During this phase, significant microscopic damage and localized plastic deformation occurred, characterized by dislocation proliferation and accumulation, which led to the development of a tensile residual stress field [26]. In subsequent fatigue stages, a marked reduction in residual stress was observed, decreasing to 21.38 MPa at 3800 cycles. Ultimately, at 4300 cycles, visible cracks appeared on the material surface, accompanied by a compressive residual stress of -12.26 MPa. This phenomenon is attributed to intense localized plastic deformation and relaxation near the crack during both initiation and propagation phases, progressively alleviating the previously accumulated tensile residual stress at the surface. Concurrently, ongoing crack propagation redistributed the internal stress field, further reducing surface tensile stress. As the crack approached penetration through the material, the crack tip region underwent substantial plastic contraction due to diminished local load-bearing capacity, resulting in the formation of a compressive residual stress field in that area [27]. Croft observed that under fatigue loading, the plastic zone ahead of the crack tip develops in conjunction with the stress intensity factor, accumulating numerous dislocations and vacancies, which contribute to the generation of residual compressive stress during crack growth [28, 29].

To further elucidate the evolution of the specimen at various stages of fatigue, this study investigated the variation in the full width at half maximum (FWHM) of X-ray diffraction peaks as a function of the number of loading cycles. As depicted in Fig. 7(b),

the initial FWHM of the specimen was measured at 1.634°. With increasing fatigue load cycles, a pronounced increase in FWHM was observed during the early and intermediate fatigue stages, reaching a peak value of 1.726° at 2200 cycles. The application of cyclic loading induces the progressive accumulation of internal micro-defects, which consequently leads to enhanced lattice distortion and broadening of the diffraction peaks. This observation is consistent with previously reported residual stress data, which indicate a concurrent increase in surface tensile residual stress during this stage, reflecting ongoing dislocation proliferation and plastic deformation. Beyond 2200 cycles, the FWHM exhibited a decreasing trend, ultimately attaining a value of 1.632° at 4300 cycles. It is hypothesized that during this phase, crack initiation and stable propagation occur, resulting in the release of localized strain energy as the plastic zone at the crack tip relaxes. This process alleviates some of the defects and residual strain initially present in the material's surface layer, thereby contributing to the observed reduction in FWHM. Simultaneously, a notable transition in residual stress from tensile to compressive states was observed prior to fracture. These findings suggest a correlation between the release of residual stress associated with crack propagation and the subsequent microstructural redistribution. Pinheiro's analysis of fatigue damage in steel pipes similarly reported an initial increase followed by a decrease in FWHM with increasing cycle number [30], corroborating the present results. Pinheiro attributed the initial FWHM increase to an escalation in dislocation density, dislocation entanglement, and the compression and intrusion of persistent slip bands. Conversely, the subsequent decrease was ascribed to dislocation rearrangement and the formation and growth of micro-cracks. Furthermore, Pinheiro identified a tertiary stage characterized by a renewed increase in FWHM for certain samples, which was linked to the generation of new free surfaces during macro-crack propagation, thereby increasing the material's stored energy. However, in the current study, measurements

were conducted proximal to the crack tip, and thus, this tertiary increase in FWHM was not observed.

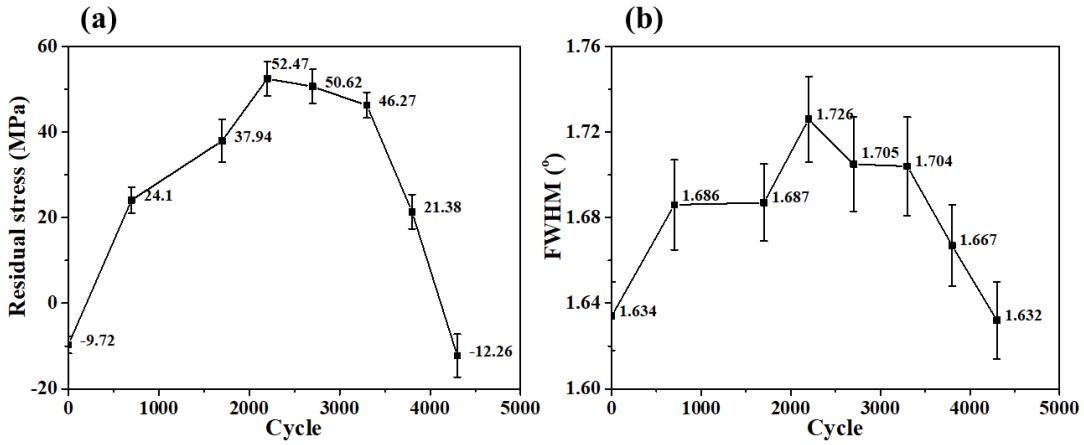


Fig. 7 (a)The residual stress, (b)the FWHM at different loading cycles.

To further investigate the relationship between the reduction in residual stress and full width at half maximum (FWHM) during fatigue, as well as the initiation and progression of surface cracks, this study performed surface optical microscopy on samples subjected to 2200, 2700, 3300, and 4300 fatigue cycles. The selection of these specific cycle counts was informed by prior analyses that identified critical inflection points or changes in residual stress, FWHM, and hardness at these stages. The results of the optical microscopy observations are presented in Fig. 8. At 2200 cycles, the samples exhibited maximum values of residual stress and FWHM, indicating that microscopic damage within the material had accumulated to a critical threshold. At this stage, suspected micro-crack contours were observable under the microscope; however, it was not definitively established whether these features represented micro-cracks or grain boundary outlines. Upon reaching 2700 cycles, both FWHM and residual stress

decreased, while hardness showed a slight increase, and distinct micro-cracks became apparent on the sample surface. By 3300 cycles, the decline in FWHM and residual stress was more pronounced, with micro-cracks evolving into macroscopic cracks, as evidenced by differences in photographic scale. Finally, at the late fatigue stage of 4300 cycles, visible macroscopic open cracks appeared on the material surface, and all previously measured metrics had decreased to their lowest values, suggesting that the material was approaching failure. These observations clearly demonstrate that, during the late stages of fatigue, the marked decline in various metrics is closely associated with the initiation and propagation of cracks.

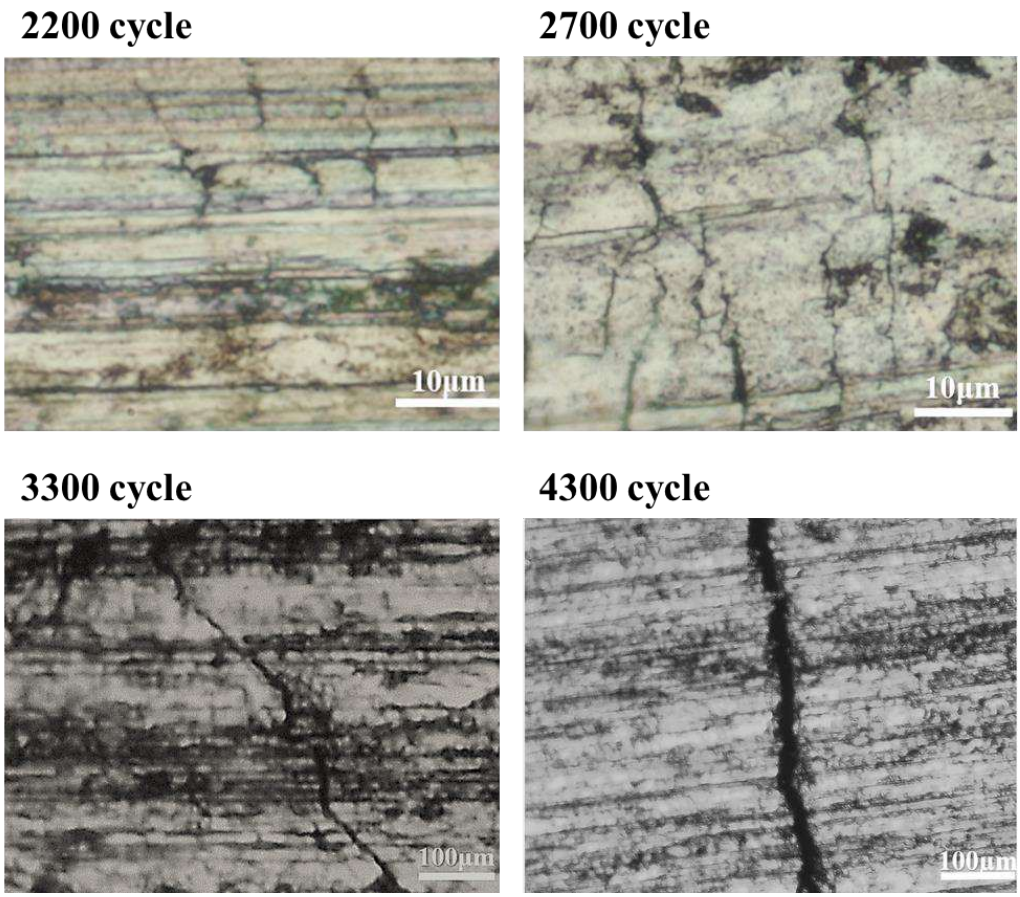


Fig. 8 The sample surface crack at different loading cycles.

To examine the microscopic damage behavior of the samples during cyclic loading, this study employed a pulse-echo ultrasonic transducer to measure changes in acoustic velocity and signal attenuation (RMS amplitude) of the specimens at various fatigue cycle stages, as depicted in Fig. 9. The initial acoustic velocity of the specimen (0 cycles) was approximately 6477 m/s, and it decreased sharply at 700 cycles, as shown in Fig. 9(a). With increasing cycle number, the acoustic velocity change was not obvious, reaching a minimum value of approximately 6362 m/s at 2200 cycles. This trend is consistent with the theoretical expression for longitudinal wave velocity V_L in materials (eq. 5):

$$v_L = \sqrt{\frac{E(1-\nu)}{\rho(1+\nu)(1-2\nu)}} \qquad \text{eq. 5}$$

where E represents the Young's modulus, ν denotes the Poisson's ratio, and ρ signifies the material density. When materials undergo repeated fatigue loading, microscopic damage—such as increased dislocation density and the initiation and propagation of microcracks—leads to a reduction in the effective elastic modulus and an increase in local inhomogeneity within the material [16, 31, 32]. This degradation further diminishes the efficiency and velocity of acoustic wave transmission. The effect of microscopic damage on material density is negligible, as fatigue damage does not cause significant volumetric changes. Therefore, the rapid decline in acoustic velocity observed during the early stages of fatigue reflects the rapid formation and accumulation of microscopic damage within the material. At 2700 cycles, a slight increase in acoustic velocity to 6390 m/s was observed; this phenomenon may be attributed to the presence of sufficient reflective interfaces generated by internal cracks, which cause premature reflection of some acoustic waves, resulting in a minor increase

in measured acoustic velocity. Subsequently, as crack propagation stabilized, the acoustic velocity slightly decreased and eventually stabilized, reaching approximately 6370 m/s prior to fracture. It should be noted that the thickness of the specimen may also vary because of the external loadings, which could be the reason why the velocity is not reliable.

The analysis of signal attenuation, as quantified by the RMS amplitude shown in Fig. 9(b), reveals that the initial RMS amplitude of the specimen was 85.06 mV. This amplitude gradually decreased with an increasing number of fatigue cycles, reaching approximately 82.52 mV at 2200 cycles. The observed reduction in amplitude is attributed to the accumulation of internal damage, including increased dislocation density and the formation of microcracks. These microstructural changes enhance the reflection and scattering of ultrasonic signals, leading to energy dissipation and a consequent decrease in amplitude [17, 23]. In the later stages of fatigue, the stable propagation of macroscopic cracks and the expansion of damaged regions further amplify the scattering and absorption of ultrasonic energy. As a result, the RMS amplitude exhibited a more pronounced decline, dropping to 63.82 mV immediately prior to fracture at 4300 cycles.

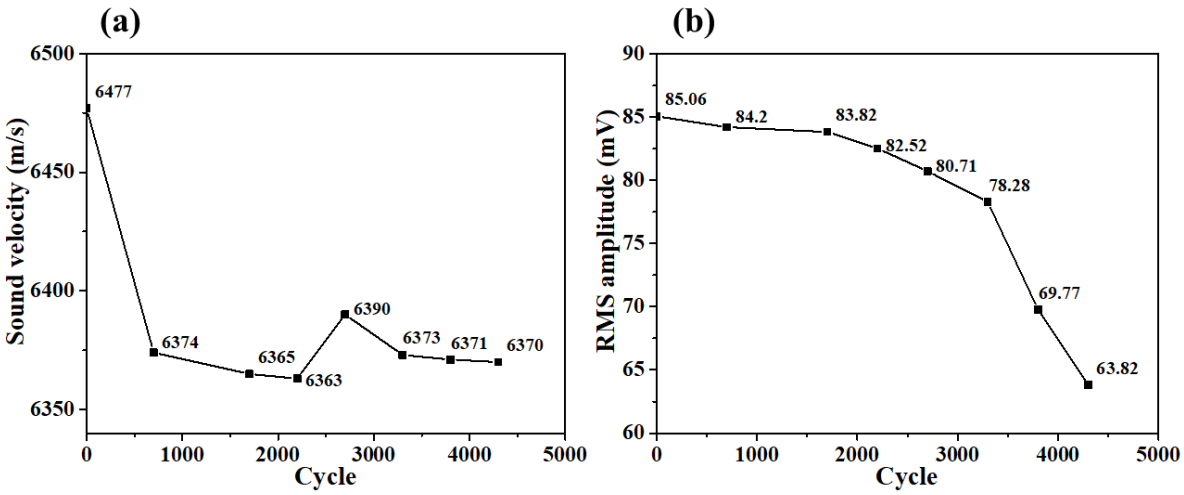


Fig. 9 (a) the acoustic velocity and (b) the RMS amplitude of the sample at different cycles.

Fig. 10(a) depicts the LCR waveforms recorded from the specimen at different fatigue cycle counts (0, 2700, and 4300 cycles). It is evident that as the number of loading cycles increases, the amplitude of the waveforms decreases significantly, accompanied by a gradual delay in the peak positions. Fig. 10(b) shows the corresponding time-of-flight (TOF) reception times for each cycle count. The TOF of the critical refracted wave in the initial state (0 cycles) is measured at 8.25 μs. With increasing fatigue cycles, the TOF demonstrates a gradual upward trend. Specifically, during the transition from early to mid-fatigue stages (0 to 2700 cycles), the TOF increases from 8.25 μs to 8.31 μs. This observation indicates the progressive accumulation of micro-damage and the development of microcracks within the specimen, which contribute to increased material inhomogeneity and impediments to acoustic wave propagation, thereby prolonging wave travel times. As fatigue progresses into the later stages (beyond 3300 cycles), the TOF values exhibit a pronounced increase, particularly as the material approaches fatigue fracture. The TOF rises sharply from 8.30 μs to a final value of 8.42 μs. This rapid escalation clearly reflects the formation and rapid growth of numerous macrocracks during the late fatigue stages. Moreover, the degradation of the specimen's lattice structure substantially impairs acoustic wave transmission efficiency, resulting in a marked reduction in wave velocity and a significant extension of arrival time.

The time of flight (TOF) of longitudinal critically refracted (LCR) waves is frequently utilized to evaluate the residual stress within a material. This assessment involves comparing the measured TOF of LCR acoustic waves to that of a stress-free

reference sample, thereby enabling the determination of the time differential [33]. An increase in this time differential is indicative of tensile stress. When the TOF data presented in Fig. 10(b) are converted into residual stress as a function of the number of loading cycles, the resulting trend closely parallels that of the TOF measurements. However, this trend significantly diverges from the residual stress results obtained via X-ray diffraction, as shown in Fig. 7(a). Specifically, after 2200 cycles, the X-ray data demonstrate a reduction in residual stress from a tensile state, whereas the LCR data continue to indicate an increase. It is important to note that the detection depth of the LCR method is approximately 1 mm beneath the surface [34], whereas X-ray stress analysis penetrates only about 10 μm. Therefore, it can be inferred that the formation of cracks at the very surface leads to the release of surface residual stress, resulting in decreased values measured by X-ray diffraction. In contrast, the absence of cracks within the bulk of the sample permits either the continued accumulation of tensile residual stress or the reduction of compressive residual stress under cyclic loading conditions.

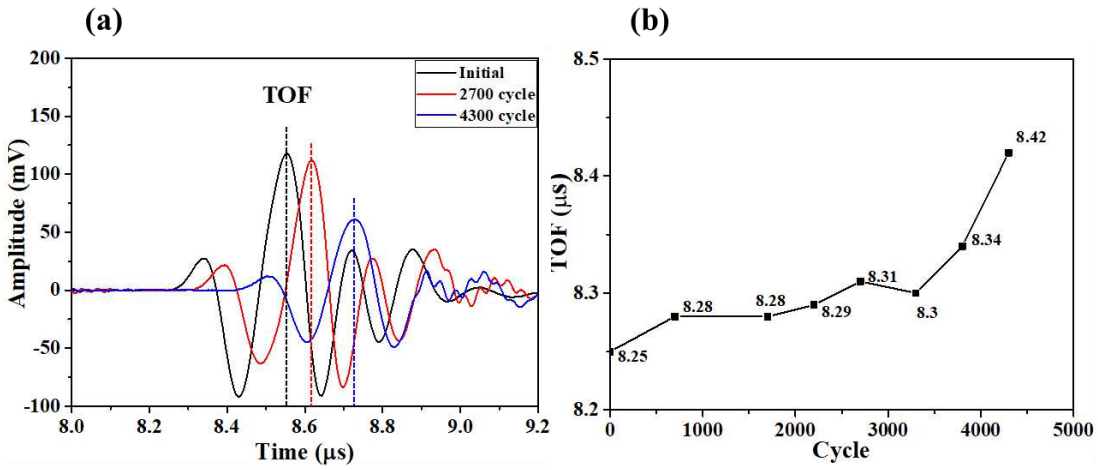


Fig. 10 (a) the illustration of TOF; (b) TOF of the sample at different loading cycles.

Fig. 11(a) illustrates the SPC curves of the specimen across various fatigue cycles, with each curve representing SPC values at distinct threshold levels. As the number of fatigue cycles increases, the SPC values demonstrate a modest upward trend, with the SPC at 3800 cycles being markedly higher than at other intervals. Upon reaching the final stage of fatigue damage (4300 cycles), the SPC value declines sharply to a level comparable to the initial state, coinciding with the appearance of visible macroscopic cracks on the specimen surface. The observed increase in SPC values throughout the fatigue process reflects the progressive intensification of internal microscopic defects and dislocation accumulation within the material, which enhances its nonlinear characteristics. Notably, even after the formation of closed-type macroscopic cracks on the surface (approximately 3300 cycles), the SPC values continue to rise. This finding suggests that closed cracks still facilitate effective nonlinear interactions during ultrasonic wave propagation, thereby increasing both the number and intensity of sideband signals. However, when fatigue damage advances to the final stage (4300 cycles) and open-type macroscopic cracks become evident on the surface, the SPC value decreases sharply to near its initial level. This pronounced reduction is attributed to substantial energy loss and reflection of ultrasonic signals caused by the open cracks, which rapidly diminish the previously prominent nonlinear sideband effects. Although the SPC value at this stage approximates the initial condition, the spectral characteristics remain significantly altered, indicating notable differences in signal distribution arising from internal material heterogeneity and crack propagation relative to the initial state.

The SPC-I was calculated from the SPC values recorded at each fatigue cycle, with the results depicted in Figure 10(b). During the initial damage phase, the SPC-I value increases rapidly, demonstrating its high sensitivity to early-stage damage. As the number of fatigue cycles increases, the SPC-I shows a gradual upward trend until the

surface exhibits visible macroscopic cracks, at which point the value decreases markedly. Notably, a significant jump in the SPC-I occur around 2200 and 2700 cycles. Previous optical microscopy analyses have identified this stage as corresponding to the initiation and progressive coalescence of microcracks. Therefore, it can be concluded that the SPC-I not only effectively reflects the progression of macroscopic crack growth but also exhibits considerable sensitivity and responsiveness to the early indicators of microcrack formation.

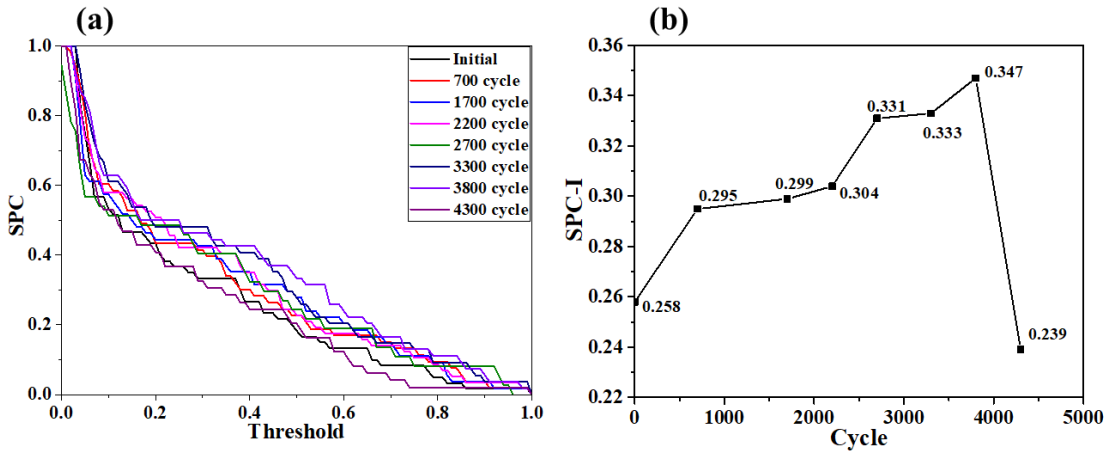


Fig. 11 (a) the SPC versus different threshold of tested sample at each loading cycles; (b) The SPC-I versus different loading cycles.

Based on the previously presented experimental results regarding residual stress and full width at half maximum (FWHM), it is evident that these two parameters are closely interrelated throughout the progression of fatigue loading. During the initial stages of fatigue, both FWHM and residual stress exhibit a gradual increase. As fatigue damage accumulates, these indicators undergo a rapid decline in the later stages of fatigue (approximately at 3,300 cycles), suggesting that under cyclic loading, the specimen transitions from initial microstructural strengthening to late-stage softening

and failure primarily driven by crack formation. However, the limited penetration depth of X-rays relative to the metal sample complicates precise monitoring of residual stress within the workpiece and also affects the accuracy of FWHM measurements. Therefore, although the analysis of these material properties offers qualitative insights into the trends observed at various fatigue stages, accurately quantifying the extent of fatigue damage remains challenging. Consequently, ultrasonic testing methods are employed to enable a more quantitative assessment of fatigue damage.

Acoustic velocity measurements indicated a significant reduction in velocity during the initial fatigue phase (700 cycles), followed by comparatively minor fluctuations in subsequent cycles. Although an increase in velocity observed at 2700 cycles suggests ongoing internal damage progression within the material, the velocity data obtained during later fatigue stages exhibited limited discriminatory power, potentially resulting in inaccurate evaluations of damage severity. Analysis of the root mean square (RMS) amplitude attenuation revealed a gradual decrease in amplitude signals, with notable changes occurring only in the advanced fatigue stage (approximately 3300 cycles), thereby indicating limited sensitivity of acoustic wave amplitude to early-stage fatigue.

The analysis of LCR wave data indicates variations in the time of flight (TOF), with the arrival time of the critical refracted wave increasing progressively as material damage intensifies. Notably, significant changes are primarily evident during the advanced stages of fatigue, around 3,300 cycles. Before the emergence of macroscopic open cracks on the material surface, SPC-I values exhibit a steady and gradual increase. Importantly, during the initial phases of the fatigue test, SPC-I shows a pronounced rapid increase, highlighting its high sensitivity to the early onset of material fatigue damage.

To further assess the sensitivity of SPC-I relative to other ultrasonic testing

methods in detecting microscopic damage, this study calculated the rate of change for each parameter relative to the initial value (0 cycles) across various ultrasonic parameters, including SPC-I values, sound velocity, RMS amplitude, and TOF. The results, presented in Fig. 12, clearly demonstrate that SPC-I exhibits a greater magnitude of change compared to the other ultrasonic analysis techniques. Moreover, analysis of the rate of change progression over different fatigue periods revealed a pronounced increase in SPC-I values at 2,200 cycles. Based on prior observations using optical microscopy, this stage corresponds to the initiation of microcracks, preceding their coalescence. Therefore, it can be inferred that the nonlinear ultrasonic analysis method SPC-I effectively detects microscopic damage within the material during the early stages of fatigue. Additionally, the maximum rate of change in SPC-I occurs at 3,800 cycles, coinciding with the formation of macroscopic cracks on the specimen surface. This finding further substantiates that SPC-I, as a nonlinear analytical method, is more sensitive and effective in detecting changes in material damage. To further elucidate the trends in the rate of change of each parameter presented in Fig. 12, the SPC-I index—exhibiting the most pronounced variation—was integrated with the microstructural evolution and schematically depicted in Fig. 13. During the initial phase characterized by the gradual accumulation of material dislocations, the rate of change of SPC-I increases slowly. As microcracks begin to form on the surface, this rate rises markedly, followed by a rapid decrease as the cracks propagate into open macroscopic fractures. These observations suggest that SPC-I is highly sensitive to early micro-damage within the material, rendering it a suitable indicator for early damage detection. Consequently, SPC-I effectively reflects the material's degradation state prior to failure and holds potential as a prognostic indicator for impending failure.

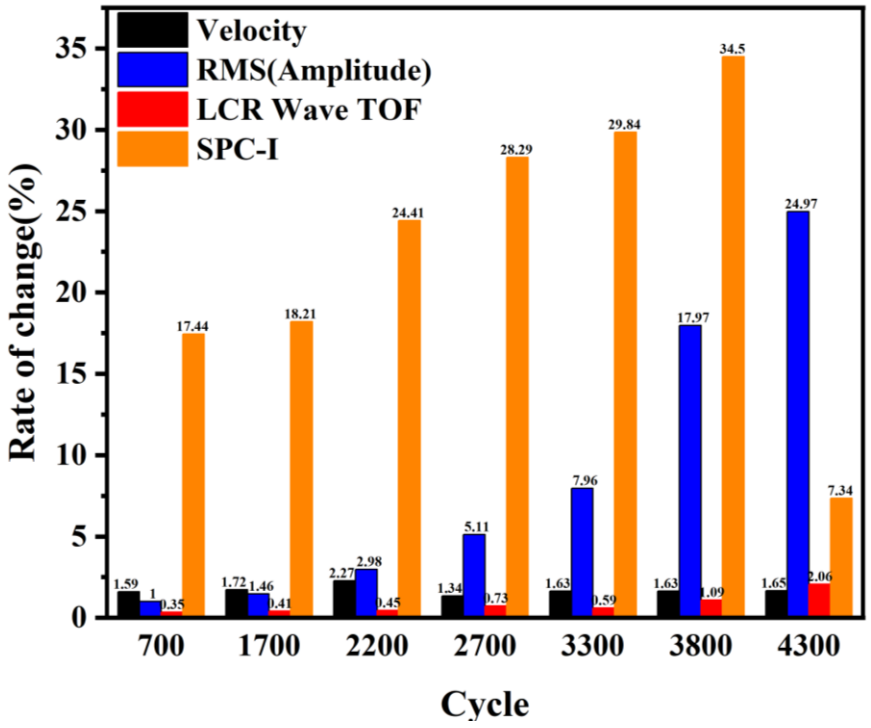


Fig. 12 Comparing the rate of change in results derived from the above analysis.

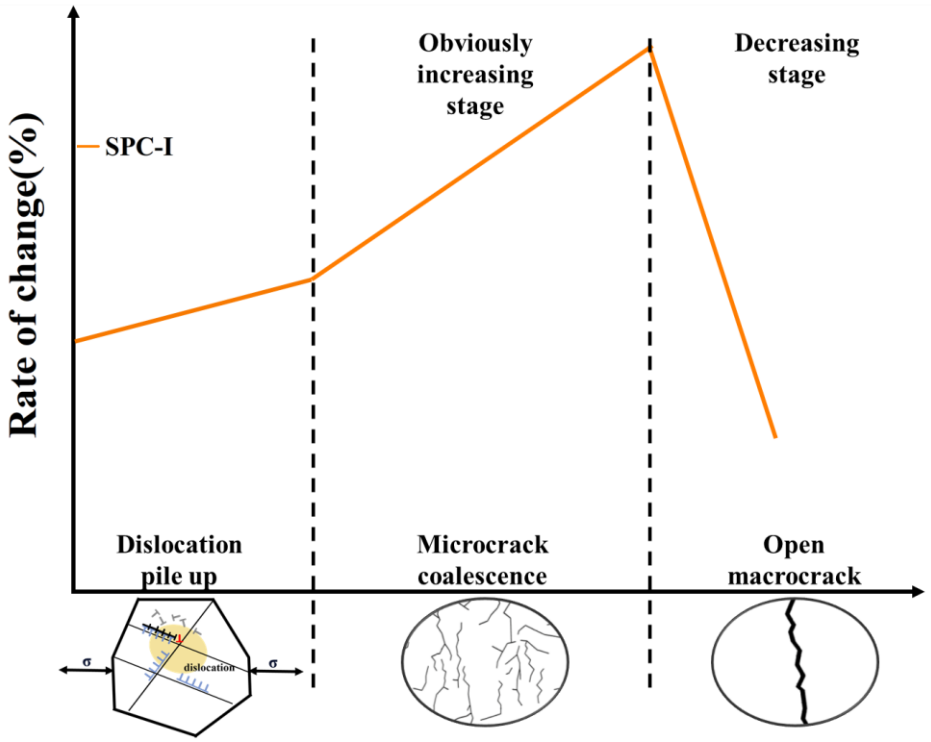


Fig. 13 Schematic diagram integrating SPC-I and microstructures.

4. Conclusions

This study utilized AA5083-H112 aluminum alloy as the experimental material and applied both linear and nonlinear ultrasonic analysis techniques to detect microscopic damage behavior preceding fatigue crack initiation. The linear ultrasonic analysis focused on acoustic velocity and root mean square (RMS) amplitude, while the nonlinear ultrasonic analysis investigated the time of flight (TOF) and sideband peak count (SPC) of the critical refracted longitudinal wave (LCR). Additionally, X-ray diffraction and microscopic optical imaging were employed to comprehensively evaluate the damage characteristics and microstructural changes of the material at various fatigue stages. Based on the experimental findings and data analysis, the following key conclusions were drawn:

1. Residual stress and the full width at half maximum (FWHM) of diffraction peaks, as determined by X-ray diffraction, varied with the number of load cycles and demonstrated significant trend changes subsequent to crack initiation. However, the limited penetration depth of X-rays into the specimen compromised the reproducibility and accuracy of the monitoring data, thereby undermining the reliability of the FWHM measurements. Moreover, the residual stress values obtained through X-ray diffraction differed markedly from those measured using the LCR method. Therefore, residual stress and FWHM are considered unsuitable parameters for monitoring fatigue crack initiation.
2. Ultrasonic acoustic velocity measurements revealed significant changes during the very first stages of fatigue; however, they showed no substantial variation with further increases in fatigue cycles. In contrast, the RMS amplitude did not immediately reflect the presence of microscopic cracks, as its rate of change became notable only when the cracks had progressed to a more advanced stage.

3. Significant changes in the time of flight (TOF) and amplitude attenuation of the LCR wave primarily occur after the formation of macroscopic cracks. Although these parameters demonstrate limited sensitivity to minor damage, they serve as reliable indicators of advanced crack development and fracture precursors, making them suitable for monitoring cracks during later stages.
4. The SPC-I showed a marked increase during the initial phase of fatigue cycling, effectively reflecting the accumulation of microscopic damage within the material. This result indicates that nonlinear ultrasonic techniques exhibit high sensitivity to early-stage fatigue damage and can provide earlier detection of damage initiation compared to conventional linear indicators.

Acknowledgements

The authors acknowledge experimental support from the National Science and Technology Council under the project “NSTC 114-2622-8-006-016” and “NSTC 114-2221-E-005 -056”.

Declaration of Interest statement

The authors declare that they have no known competing financial interests or personal relationships that could have appeared to influence the work reported in this paper.

Data Availability

The authors confirm that the data supporting the findings of this study are available within the article.

Reference

1. Campbell FC. Elements of Metallurgy and Engineering Alloys. Materials Park, Ohio: ASM International; 2008.
2. Mix PE. Introduction to Nondestructive Testing: A Training Guide. 2nd ed. New Jersey, USA: John Wiley & Sons; 2005.
3. Alnuaimi H, Amjad U, Russo P, Lopresto V, Kundu T (2021) Monitoring damage in composite plates from crack initiation to macro-crack propagation combining linear and nonlinear ultrasonic techniques. Struct Health Monit 20(1):139–50. doi: https://doi.org/10.1177/1475921720922922.
4. Tian F, Hao Y, Zou Z, Zheng Y, He W, Yang L, et al. (2019) An ultrasonic pulse-echo method to detect internal defects in epoxy composite insulation. Energies 12(24):4804.
5. Sohn H (2011) Reference-free crack detection under varying temperature. KSCE J Civ Eng 15(8):1395–404. doi: https://doi.org/10.1007/s12205-011-1271-0.
6. Lissenden CJ (2021) Nonlinear ultrasonic guided waves—Principles for nondestructive evaluation. J Appl Phys 129(2):021101. doi: https://doi.org/10.1063/5.0038340.
7. Hikata A, Elbaum C (1966) Generation of ultrasonic second and third harmonics due to dislocations. I. Phys Rev 144(2):469–77. doi: https://doi.org/10.1103/PhysRev.144.469.
8. Buck O, Morris WL, Richardson JM (1978) Acoustic harmonic generation at unbonded interfaces and fatigue cracks. Appl Phys Lett 33(5):371–3. doi: https://doi.org/10.1063/1.90399.
9. Jhang K-Y, Kim K-C (1999) Evaluation of material degradation using nonlinear acoustic effect. Ultrasonics 37(1):39–44. doi: https://doi.org/10.1016/S0041-624X(98)00045-6.
10. Van Den Abeele KEA, Johnson PA, Sutin A (2000) Nonlinear elastic wave spectroscopy (NEWS) techniques to discern material damage, part I: nonlinear wave modulation spectroscopy (NWMS). Res Nondestr Eval 12(1):17–30. doi: https://doi.org/10.1080/09349840009409646.
11. Chen XJ, Kim JY, Kurtis KE, Qu J, Shen CW, Jacobs LJ (2008) Characterization of progressive microcracking in Portland cement mortar using nonlinear ultrasonics. NDT & E Int 41(2):112–8. doi: https://doi.org/10.1016/j.ndteint.2007.08.009.
12. Sohn H, Lim HJ, DeSimio MP, Brown K, Derriso M (2014) Nonlinear ultrasonic wave modulation for online fatigue crack detection. J Sound Vibrat 333(5):1473–84. doi: https://doi.org/10.1016/j.jsv.2013.10.032.
13. Geimer PR, Beardslee L, Ulrich TJ (2023) Nonlinear resonant ultrasound spectroscopy using white-noise excitation. J Acoust Soc Am 154(4_supplement):A67–A. doi: https://doi.org/10.1121/10.0022818.
14. Chavazas M-L, Bromblet P, Berthonneau J, Hénin J, Payan C (2024) Impact of

relative humidity variations on Carrara marble mechanical properties investigated by nonlinear resonant ultrasound spectroscopy. Constr Build Mater 431:136529. doi: https://doi.org/10.1016/j.conbuildmat.2024.136529.
15. Shokouhi P, Riviere J (2021) Nonlinear resonant ultrasound spectroscopy (NRUS) for nondestructive evaluation. J Acoust Soc Am 150(4_Supplement):A40–A. doi: https://doi.org/10.1121/10.0007554.
16. Oruganti RK, Sivaramanivas R, Karthik TN, Kommareddy V, Ramadurai B, Ganesan B, et al. (2007) Quantification of fatigue damage accumulation using non-linear ultrasound measurements. Int J Fatigue 29(9):2032–9. doi: https://doi.org/10.1016/j.ijfatigue.2007.01.026.
17. Sun D, Zhu W, Qiu X, Liu L, Xiang Y, Xuan F-Z (2023) Nonlinear ultrasonic detection of closed cracks in metal plates with phase-velocity mismatching. NDT & E Int 135:102788. doi: https://doi.org/10.1016/j.ndteint.2023.102788.
18. Park S, Bokhari I, Alnuaimi H, Amjad U, Fleischman R, Kundu T (2025) Early detection of steel tube welded joint failure using SPC-I nonlinear ultrasonic technique. Struct Health Monit 24(1):148–63. doi: https://doi.org/10.1177/14759217241235057.
19. Alnuaimi HN, Amjad U, Russo P, Lopresto V, Kundu T (2025) Advanced non-linear ultrasonic sideband peak count-index technique for efficient detection and monitoring of defects in composite plates. J Vibrat Control 31(3-4):221–33. doi: https://doi.org/10.1177/1077546323116822.
20. Park S, Kundu T (2023) A modified sideband peak count based nonlinear ultrasonic technique for material characterization. Ultrasonics 128:106858. doi: https://doi.org/10.1016/j.ultras.2022.106858.
21. Kundu T, Eiras JN, Li W, Liu P, Sohn H, Payá J (2019) Fundamentals of Nonlinear Acoustical Techniques and Sideband Peak Count. In: Kundu T, editor. Nonlinear Ultrasonic and Vibro-Acoustical Techniques for Nondestructive Evaluation. Cham: Springer International Publishing. p. 1–88.
22. Castellano A, Fraddosio A, Piccioni MD, Kundu T (2021) Linear and Nonlinear Ultrasonic Techniques for Monitoring Stress-Induced Damages in Concrete. J Nondestr Eval Diag 4(4):041001. doi: https://doi.org/10.1115/1.4050354.
23. Zhang G, Li X, Li T, Kundu T (2023) Monitoring elastoplastic deformation in ductile metallic materials using sideband peak count-index technique. J Nondestr Eval Diag 6(3):031004. doi: https://doi.org/10.1115/1.4062930.
24. dos Santos AA, Jr., Bray DE (2002) Comparison of acoustoelastic methods to evaluate stresses in steel plates and bars. J Press Vessel Technol 124(3):354–8. doi: https://doi.org/10.1115/1.1484114.
25. Lai H-H, Wu W (2020) Practical examination of the welding residual stress in view of low-carbon steel welds. J Mater Res Technol 9(3):2717–26. doi:

https://doi.org/10.1016/j.jmrt.2020.01.004.
26. Weiss V, Oshida Y, Wu A (1980) A note on fatigue damage assessment by x-ray diffraction techniques for a 304L stainless steel specimen. J Nondestr Eval 1(3):207–13. doi: https://doi.org/10.1007/BF00567093.
27. Belnoue JP, Jun T-S, Hofmann F, Abbey B, Korsunsky AM (2010) Evaluation of the overload effect on fatigue crack growth with the help of synchrotron XRD strain mapping. Eng Fract Mech 77(16):3216–26. doi: https://doi.org/10.1016/j.engfracmech.2010.08.018.
28. Croft M, Shukla V, Jisrawi NM, Zhong Z, Sadangi RK, Holtz RL, et al. (2009) Mapping and load response of overload strain fields: Synchrotron X-ray measurements. Int J Fatigue 31(11):1669–77. doi: https://doi.org/10.1016/j.ijfatigue.2009.01.020.
29. Croft MC, Jisrawi NM, Zhong Z, Holtz RL, Sadananda K, Skaritka JR, et al. (2007) Fatigue history and in-situ loading studies of the overload effect using high resolution X-ray strain profiling. Int J Fatigue 29(9):1726–36. doi: https://doi.org/10.1016/j.ijfatigue.2007.01.016.
30. Pinheiro B, Lesage J, Pasqualino I, Bemporad E, Benseddiq N (2013) X-ray diffraction study of microstructural changes during fatigue damage initiation in pipe steels: Role of the initial dislocation structure. Mater Sci Eng, A 580:1–12. doi: https://doi.org/10.1016/j.msea.2013.05.042.
31. Kumar A, Torbet CJ, Pollock TM, Wayne Jones J (2010) In situ characterization of fatigue damage evolution in a cast Al alloy via nonlinear ultrasonic measurements. Acta Mater 58(6):2143–54. doi: https://doi.org/10.1016/j.actamat.2009.11.055.
32. Kabatova M, Dudrova E, Wronski AS (2009) Microcrack nucleation, growth, coalescence and propagation in the fatigue failure of a powder metallurgy steel. Fatigue Fract Eng Mater Struct 32(3):214–22. doi: https://doi.org/10.1111/j.1460-2695.2009.01328.x.
33. Lai H-H, Yan D-H, Chang W-J, Chung K-H, Xing L-X, Chang W-T, et al. (2024) Effects of factors from practical workpieces on ultrasonic LCR method stress measurement. Discov Appl Sci 6(7):335. doi: https://doi.org/10.1007/s42452-024-06003-z.
34. Javadi Y, Hloch S (2013) Employing the L_{CR} waves to measure longitudinal residual stresses in different depths of a stainless steel welded plate. Adv Mater Sci Eng 2013(1):746187. doi: https://doi.org/10.1155/2013/746187.